Elasticity of Confined Simple Fluids from an Extended Peng-Robinson Equation of State

Santiago A. Flores Roman,† Gabriel D. Barbosa,‡ and Gennady Y. Gor*,†

†Otto H. York Department of Chemical and Materials Engineering,

New Jersey Institute of Technology, University Heights, Newark, NJ 07102, USA

‡Department of Chemical and Biological Engineering,

The University of Alabama, Tuscaloosa, AL 35487, USA

E-mail: gor@njit.edu

Abstract

Thermodynamic properties of fluids in nanopores are altered by confinement, and equations of state (EOS) for bulk fluids are not able to predict them. We utilized a recent EOS based on the Peng-Robinson EOS, which takes into account the effects of confinement, to derive an analytical expression for the elastic properties of the fluid, isothermal bulk modulus, or compressibility. We calculated the modulus of liquid argon confined in model spherical nanopores of various sizes. We compared the predictions based on the EOS to calculations of the bulk modulus directly from Monte Carlo simulations in the grand canonical ensemble (GCMC). The bulk modulus of argon in mesopores predicted by the EOS appeared consistent with the GCMC predictions, showing in particular linear dependence on Laplace pressure and on the inverse pore size. Furthermore, the EOS appeared capable of predicting the modulus of the fluid in micropores, where GCMC predictions failed. Our result is a step towards developing an equation of state for confined fluids, which can be used for predictions of elasticity.

Keywords: Confined fluid, Equation of state, Compressibility, Elastic Modulus

Introduction

Predicting the behavior of confined fluids in nanopores is needed for many science and engineering applications. Examples include nanofluidic devices, ^{1,2} electrochemical applications, ^{3–5} and even water in nanopores inside the collagen-apatite matrix in bones, ⁶ etc. However, within the last decade, the interest in confined fluids has been strongly driven by the exploration and development of unconventional hydrocarbon resources. ^{7–11} Several experimental and theoretical studies demonstrated that the elasticity (bulk modulus or compressibility) of confined hydrocarbons differs from the elasticity of the same fluid in bulk. ^{12–15} The elasticity of fluids in the pores contributes to the elasticity of the fluid-saturated porous media, which determines the speed of seismic waves and is needed for the correct interpretation of seismic data used for geophysical exploration. ^{16–18} Therefore, quantitative predictions for the elasticity of a confined fluid are of practical interest.

The elastic modulus of confined fluids can be theoretically predicted by using methods based on statistical mechanics. For example, molecular dynamics, ^{14,19} Monte Carlo simulations, ^{15,20} and classical density functional theory (cDFT). ^{21–23} Nevertheless, depending on the system, simulations may require high computational resources to predict elasticity with high enough accuracy. Regarding cDFT, its applicability for confined systems is limited to simple fluids, ²⁴ and even for them, cDFT fails to provide quantitative predictions. ²⁵ Alternatively, the elastic modulus of a confined fluid, similar to a bulk fluid, can be calculated based on an equation of state (EOS). ²⁶

EOSs have the advantage of containing the whole system's thermodynamics in a set of equations, so it is enough to know some system's variables according to the degrees of freedom of the fluid to describe its state completely. One of the simplest EOSs developed for real liquids is the van der Waals EOS (vdW EOS), ²⁷ from which several EOSs were derived to describe confined fluids: Schoen and Diestler extended the vdW EOS utilizing perturbation theory, ²⁸ Truskett et al. used Schoen and Diestler's approach to include hydrogen-bonding interactions, ²⁹ Zarragoicoechea and Kuz applied classical thermodynamics, and stress tensors

instead of perturbations, 30 and Travalloni et al. extended the vdW EOS through density packing (TvdW EOS). 31

Even though none of the equations mentioned previously were developed focusing on calculating the elasticity of confined fluids, Dobrzanski et al. succeeded in deriving the isothermal elastic modulus from the TvdW EOS and utilized it for predicting confined argon in cylindrical silica pores. ²⁶ TvdW EOS succeeded in predicting only qualitatively capillary condensation, the adsorbed amount of molecules on the pore, and elasticity. One possible cause of this disagreement is the vdW EOS chosen as a basis since it can only qualitatively predict the properties of bulk fluids. Instead, Peng-Robinson EOS (PR EOS) ³² can predict elasticity for the bulk phase with reasonable accuracy. To improve TvdW EOS, Barbosa et al. extended the PR EOS using the same approach as Travalloni et al. did for their EOS and generalized it to spherical and cylindrical pores. ³³

In the current paper, we derived analytical expressions that calculate the elastic modulus of fluids from an EOS developed by Barbosa et al. (we will refer to it as BPR, for short). We parameterized BPR EOS based on the data for argon in spherical silica pores generated from Monte Carlo molecular simulations in the grand canonical ensemble (GCMC). We used the resulting parameters to calculate elasticity from BPR EOS and compared it to the calculations based on GCMC. Our results showed significant improvement compared to the earlier results by Dobrzanski et al., ²⁶ based on the TvdW EOS. ³¹

Methods

Below is a detailed description of the methods to model argon adsorbed on silica pores, BPR EOS, and GCMC simulations. The former method applies two assumptions to derive the coming equations: A molecule-molecule interaction potential of the square-well type and the packing of hard spheres. From these two assumptions and using the PR EOS to relate confined and bulk phases, it is possible to derive a pressure equation and a chemical potential.

The rest of the equations are implications of these assumptions. The latter method, unlike BPR EOS, utilizes Lennard-Jones (LJ) interactions for fluid-fluid and solid-fluid interactions. The chemical potential was approximated to the chemical potential of the ideal gas, and the bulk modulus was calculated from statistical mechanics.

Equation of state

Barbosa et al. derived an EOS based on the canonical ensemble and assumed that fluid-fluid and solid-fluid interactions are of the square-well potential type, i.e.,

$$u_{ij}(r_{ij}) = \begin{cases} \infty, & r_{ij} \le \sigma \\ -\epsilon, & \sigma < r_{ij} \le \sigma + \delta \\ 0, & r_{ij} > \sigma + \delta, \end{cases}$$
 (1)

for fluid-fluid interactions, and

$$u_i(r_i) = \begin{cases} \infty, & r_i \ge r_{\rm p} - \sigma_{\rm p}/2 \\ -\epsilon_{\rm p}, & r_{\rm p} - \sigma_{\rm p}/2 - \delta_{\rm p} \le r_i < r_{\rm p} - \sigma_{\rm p}/2 \\ 0, & r_i < r_{\rm p} - \sigma_{\rm p}/2 - \delta_{\rm p}, \end{cases}$$
(2)

for solid-fluid interactions, where r_{ij} is the distance between two fluid molecules, r_i the radial position of a fluid molecule in the pore, r_p is the external pore radius, δ and δ_p are the widths of the square-well potentials for fluid-fluid and solid-fluid interactions, respectively, and ϵ , ϵ_p , σ and σ_p are the depths and molecular diameters of their respective potentials.

Since BPR EOS is focused only on the fluid molecules, it is important to distinguish between the pore radius of the confined fluid r_{int} (also called internal pore radius) and the external pore radius. For a solid-fluid square-well potential, interactions tend to infinity for

distances between solid and fluid molecules lower than $\sigma_p/2$, hence

$$r_{\rm int} = r_{\rm p} - \frac{\sigma_{\rm p}}{2}.\tag{3}$$

For a spherical pore shape and taking as a basis the PR EOS to describe the fluid's properties in the bulk phase, for a simple and homogeneous fluid at a fixed temperature, the derived pressure equation and chemical potential are

$$P(v) = \frac{RT}{v - b_{\rm p}} - \frac{a_{\rm p}}{v(v + b_{\rm p}) + b_{\rm p}(v - b_{\rm p})} - \frac{\theta b_{\rm p} \xi}{v^2} \left(1 - \frac{b_{\rm p}}{v}\right)^{\theta - 1},\tag{4}$$

and

$$\mu(\rho) = \mu_0 + RT \left[\ln \left(\frac{\rho - \rho_{\text{max}}}{\rho} \right) + \frac{\rho}{\rho_{\text{max}} - \rho} \right]$$

$$+ \xi \left[1 - \frac{(\theta + 1)\rho}{\rho_{\text{max}}} \right] \left(1 - \frac{\rho}{\rho_{\text{max}}} \right)^{\theta - 1} - a_{\text{p}} \rho_{\text{max}} \zeta - N_{\text{A}} F_{\text{pr}} \epsilon_{\text{p}},$$
(5)

which approximate to PR EOS and its chemical potential when $r_p \to \infty$. For the rest of the parameters and variables,

$$\xi \equiv (1 - F_{\rm pr}) \left\{ RT \left[1 - \exp\left(-\frac{N_{\rm A}\epsilon_{\rm p}}{RT}\right) \right] - N_{\rm A}\epsilon_{\rm p} \right\},\tag{6}$$

$$\zeta \equiv \frac{\sqrt{2}}{4} \ln \left[\frac{\rho_{\text{max}} + (\sqrt{2} + 1)\rho}{\rho_{\text{max}} - (\sqrt{2} - 1)\rho} \right] + \frac{1}{\frac{\rho_{\text{max}}}{\rho} + 2 - \frac{\rho}{\rho_{\text{max}}}}, \tag{7}$$

$$\sigma = \frac{c_1 b}{N_{\rm A}},\tag{8}$$

 μ_0 is the reference chemical potential, v is the confined molar volume, $\rho = 1/v$ the molar density, P the fluid's pressure, T its temperature, R is the gas constant, N_A the Avogadro number, $b_p = N_A/\rho_{\rm max}$ and $a_p = ah$ the modified PR EOS parameters (a and b), $h = N_{\rm c,max}/10$, θ is a term that modulates the effect of the confined density on the fraction of

molecules in the square-well region of the pore,

$$\theta = \frac{r_{\text{int}}}{\delta_{\text{p}} + \sigma/2},\tag{9}$$

 $F_{\rm pr}$ is the fraction of the confined molecules in the same square-well region for a random distribution of the fluid,

$$F_{\rm pr} = \frac{(r_{\rm int} - \sigma/2)^3 - (r_{\rm int} - \sigma/2 - \delta_{\rm p})^3}{(r_{\rm int} - \sigma/2)^3},\tag{10}$$

 $N_{
m c,max}$ is the average molecule-molecule coordination number in the packed structure,

$$N_{\text{c,max}} = A + \frac{10 - A}{\left\{1 + U \exp\left[-B\left(\frac{r_{\text{int}}}{\sigma} - M\right)\right]\right\}^{1/\nu}} - \frac{\exp\left[-\frac{(r_{\text{int}}/\sigma - \eta)^2}{2\varphi^2}\right]}{\sqrt{2\pi}\varphi}, \quad (11)$$

 $\rho_{\rm max}$ is the molecular density of the closed-packed fluid,

$$\rho_{\text{max}}\sigma^3 = c_1 - c_2 \exp\left[c_3 \left(\frac{1}{2} - \frac{r_{\text{int}}}{\sigma}\right)\right] + c_4 \exp\left[c_5 \left(\frac{1}{2} - \frac{r_{\text{int}}}{\sigma}\right)\right],\tag{12}$$

and $c_1 = 1.095$, $c_2 = 1.127$, $c_3 = 1.562$, $c_4 = 1.942$, $c_5 = 27.456$, $A = -4.6849 \times 10^{-4}$, B = 0.2628, U = 3.3445, M = -0.8141, $\nu = 3.2547 \times 10^{-4}$, $\eta = 1.7948$, and $\varphi = 0.2666$ are universal parameters for spherical pores obtained by fitting the packed density and eq. 11 with available data.³⁴

From BPR EOS, one can derive the bulk modulus using its definition from thermody-

namics, getting

$$K_{T} \equiv -v \left(\frac{\partial P}{\partial v}\right)_{T}$$

$$= \frac{vRT}{(v - b_{p})^{2}} - \frac{2a_{p}v(v + b_{p})}{\left[v\left(v + b_{p}\right) + b_{p}\left(v - b_{p}\right)\right]^{2}}$$

$$+ \frac{\theta b_{p}}{v^{2}} \xi \left(1 - \frac{b_{p}}{v}\right)^{\theta - 2} \left[2 - \frac{b_{p}}{v}\left(\theta - 1\right)\right]. \tag{13}$$

It is important to note that we are assuming an isotropic pressure in the confined phase to allow the derivation of Eq. 13, even though the fluid-pore interactions force the fluid to become inhomogeneous. The reason to consider this assumption, further than the sake of simplicity, is that several models that were developed to predict the bulk modulus of a simple confined fluid and ignored its inhomogeneity succeeded in reasonably predicting its elastic properties. ^{14,26,35}

Solving the equation of state for confined fluids

At constant temperature, Eq. 13 is written as a function of v, where v depends on a given value of the chemical potential, i.e., $v = v(\mu)$, where $1/v = \rho$, and it gives an adsorption isotherm. To calculate it, one needs to use the equation for chemical equilibrium between the bulk and confined phases,

$$\mu_{\text{bulk}}(P_{\text{bulk}}; a, b) = \mu_{\text{conf}}(\rho, r_{\text{int}}; a, b, \epsilon_{\text{p}}, \delta_{\text{p}}). \tag{14}$$

It is easy to find the left-hand side of Eq. 14 since it depends on the Peng-Robinson parameters a and b, and the bulk pressure P_{bulk} is an arbitrary variable. Furthermore, Eq. 5 approximates the chemical potential of the PR EOS when $r_{\text{p}} \to \infty$.

To find the right-hand side of Eq. 14, the parameters $\epsilon_{\rm p}$ and $\delta_{\rm p}$ must be known in advance. One can determine these two parameters by fitting adsorption isotherms from molecular simulation data through the least squares method. For this purpose, the optimization model utilized was Particle Swarm Optimization.³⁶ Eq. 14 is complex enough to solve analytically for ρ . However, it is possible to find the derivative of the chemical potential with respect to the confined density analytically,

$$\left(\frac{\mathrm{d}\mu}{\mathrm{d}\rho}\right)_{T} = \frac{RT}{\rho^{3} \left(\frac{1}{\rho} - \frac{1}{\rho_{\mathrm{max}}}\right)^{2}} - \frac{2a_{\mathrm{p}}\rho_{\mathrm{max}}^{3} \left(\rho + \rho_{\mathrm{max}}\right)}{\left(\rho^{2} - 2\rho\rho_{\mathrm{max}} - \rho_{\mathrm{max}}^{2}\right)^{2}} + \xi\theta \left(1 - \frac{\rho}{\rho_{\mathrm{max}}}\right)^{\theta} \frac{\rho - 2\rho_{\mathrm{max}} + \theta\rho}{\left(\rho - \rho_{\mathrm{max}}\right)^{2}}, \tag{15}$$

and utilize numerical methods, such as Newton-Raphson, to solve Eq. 14. It is important to note that the BPR EOS is not a cubic EOS. Therefore, more than three solutions can be obtained by solving Eq. 14. Additionally, the number of physically meaningful roots obtained from Eq. 14 depends on the specific thermodynamic conditions and values of the BPR EOS parameters, as discussed by Travalloni et al.³¹ To identify the most stable state, we utilized the thermodynamic stability criterion, which is, for a simple homogeneous fluid in open rigid walls that interacts with a heat bath, the pressure of the confined fluid reaches its maximum at the equilibrium. The algorithm and the criterion are explained in more detail in the next section.

Calculation of adsorption isotherms from BPR EOS

The roots of Eq. 14 can be found using the Newton-Raphson method. To have a good estimate of a root, it's useful to create a grid over the range of relative densities $0 < \rho_r < 1$,

where $\rho_{\rm r} \equiv \rho/\rho_{\rm max}$. Introducing

$$\Delta \rho_{\rm r} \equiv \frac{1-\delta}{N}, \quad \delta \ll 1,$$
 (16)

$$\rho_{\mathbf{r},i} \equiv \delta + i\Delta \rho_{\mathbf{r}}, \quad \forall i \in \{0, 1, ..., N - 1\},$$
(17)

$$f(\rho_{\rm r}) \equiv \mu_{\rm conf}(\rho_{\rm r}) - \mu_{\rm bulk},$$
 (18)

$$D_{\rho_{\rm r}}[\mu_{\rm conf}(\rho_{\rm r,i})] \equiv \frac{\mathrm{d}\mu_{\rm conf}}{\mathrm{d}\rho_{\rm r}} \Big|_{\rho_{\rm r}=\rho_{\rm r,i}},\tag{19}$$

Here, N is the number of boxes that form the relative density grid, $\Delta \rho_{\rm r}$ is its uniform width, $\rho_{\rm r,i}$ is a given value among the range of relative densities, δ is a very small number, f comes from Eq. 14, and $D_{\rho_{\rm r}}[\mu_{\rm conf}]$ is Eq. 15. The absolute value of a variable x will be defined as abs(x).

The problem, therefore, becomes to find the roots of $\mu = \mu(\rho_r)$. We utilized the following algorithm.

- 1. Define $i \equiv 0$ and $tol \ll 1$.
- 2. If i = N, stop the algorithm. Otherwise, define

$$\rho_{\rm r,-\frac{1}{2}i} \equiv \rho_{\rm r,i} - 0.5\Delta\rho_{\rm r}$$

$$\rho_{\mathrm{r},+\frac{1}{2}\mathrm{i}} \equiv \rho_{\mathrm{r},i} + 0.5\Delta\rho_{\mathrm{r}},$$

and

$$f_{-\frac{1}{2}i} \equiv f(\rho_{\mathrm{r},-\frac{1}{2}\mathrm{i}})$$

$$f_{+\frac{1}{2}i} \equiv f(\rho_{\mathrm{r},+\frac{1}{2}\mathrm{i}}).$$

3. If $\left(f_{-\frac{1}{2}i}\right)\left(f_{+\frac{1}{2}i}\right) \geq 0$, define i=i+1. and go back to step 2. Otherwise, proceed to the next step.

- 4. Define $err \equiv 1$, and $\rho_{r,new} \equiv 0$. Note: err > tol.
- 5. If $err \geq tol$, then define

$$ho_{\mathrm{r,new}} =
ho_{\mathrm{r},i} - rac{f(
ho_{\mathrm{r},i})}{D_{
ho_{\mathrm{r}}}[\mu_{\mathrm{conf}}(
ho_{\mathrm{r},i})]}$$

and proceed to the following step. Otherwise, select $\rho_{r,new}$ as a root, define i = i + 1, and go back to step 2.

- 6. Define $err = abs(\rho_{r,i} \rho_{r,new})$.
- 7. Define $\rho_{r,i} = \rho_{r,new}$, and go back to step 5.

Once all the possible relative densities are found, the applicability of the stability criterion for this system will highlight the thermodynamically stable root among the rest. It is enough to choose the root that returns the highest pressure from Eq. 4, and which derivative, Eq. 15, is positive,

$$\left(\frac{\mathrm{d}\mu}{\mathrm{d}\rho}\right)_T > 0. \tag{20}$$

Stability criterion

For a simple and homogeneous fluid in rigid walls, in which temperature, the total volume of the adsorbed phase (V), and chemical potential are specified, the second law of thermodynamics renders

$$d(U - TS - \mu n) \le 0, (21)$$

where U, S, and n are the internal energy, entropy, and adsorbed fluid mole number, respectively, and the quantity in parenthesis is the well-known grand potential ($\Omega \equiv \Omega(\mu, V, T)$). Recognizing that Ω is a first-order homogeneous function in V or the Gibbs free energy $G = \mu n = U + PV - TS$, 37,38 Eq. 21 becomes $dP \ge 0$, which means that, for fluid in an open system that interacts with a heat bath and volume V (grand canonical ensemble), the thermodynamic equilibrium will be reached after maximizing the fluid's pressure.

Moreover, from the chemical potential for a simple and homogeneous fluid,

$$d\mu = -sdT + vdP, (22)$$

the following equation can be derived for thermodynamic processes at constant temperature,

$$\left(\frac{\partial \mu}{\partial \rho}\right)_T = v \left(\frac{\partial P}{\partial \rho}\right)_T. \tag{23}$$

As the pressure is a monotonic function with respect to the confined density, the term at the left side of the equality must be monotonic as well, i. e.,

$$\left(\frac{\partial \mu}{\partial \rho}\right)_T > 0. \tag{24}$$

Simulation details

Adsorption of argon was simulated on a spherical pore composed of silica for three different sizes, 1 nm, 3 nm, and 5 nm, and at the temperatures 87.3 K, 100 K, and 119.6 K for each pore size. Simulations were performed in a grand canonical ensemble using Chainbuild molecular simulation code³⁹ for a conventional GCMC method with 8×10^9 Monte Carlo trial moves. The pair potential used for fluid-fluid and solid-fluid interactions was of the LJ type, and its parameters are listed in Table 1.

Table 1: LJ parameters for confined argon on GCMC simulations (ε and σ), solid surface density ($n_{\rm s}$) and cut-off radius ($r_{\rm cut}$). 40,41 No tail corrections were used.

	$\varepsilon/k_{\rm B},{ m K}$	σ , nm	$n_{\rm s},{\rm nm}^{-2}$	$r_{ m cut},\sigma_{ m ff}$
Ar-Ar	119.6	0.34		5
Ar-Silica	171.4	0.3	15.3	10

Given the system's conditions, argon exhibits very similar behavior to that of an ideal gas, so the external pressure was related to the chemical potential through the equation

$$\mu = \mu_0 + RT \ln \left(\frac{p}{p_0}\right),\tag{25}$$

where p/p_0 is the relative pressure of the bulk fluid, and μ_0 the chemical potential at saturation pressure, which was obtained through the Johnson et al. equation of state, ⁴² $\mu_0/k_B = -1147.4 \,\mathrm{K}$. The chemical potentials were calculated under the interval of relative pressures [10⁻², 1].

For the solid-fluid interactions, we used the integrated LJ potential for a spherical pore, ⁴³

$$u_{\rm sf}(r, r_{\rm p}) = \frac{4}{5} \pi n_{\rm s} \varepsilon_{\rm sf} \sigma_{\rm sf}^{6}$$

$$\times \left\{ \sigma_{\rm sf}^{6} \sum_{i=0}^{9} \frac{1}{r_{\rm p}^{i}} \left[\frac{1}{(r_{\rm p} - r)^{10-i}} + \frac{1}{(r_{\rm p} + r)^{10-i}} \right] - \sum_{i=0}^{3} \frac{1}{r_{\rm p}^{i}} \left[\frac{1}{(r_{\rm p} - r)^{4-i}} + \frac{1}{(r_{\rm p} + r)^{4-i}} \right] \right\},$$

$$(26)$$

where $\sigma_{\rm sf}$ and $\varepsilon_{\rm sf}$ are shown in Table 1, and the internal diameter, unlike BPR EOS, is related to the former through the following equation, ⁴⁴

$$d_{\text{int}} = d_{\text{ext}} - 1.7168\sigma_{\text{sf}} + \sigma_{\text{ff}}. \tag{27}$$

For the calculation of the bulk modulus, the formulation derived from statistical mechanics was used, which requires a normal distribution of molecules during the simulation, and after thermalization,

$$K_T = \frac{1}{\beta_T} = \frac{k_{\rm B} T \langle N \rangle^2}{V \langle \delta N^2 \rangle},\tag{28}$$

where β_T is the isothermal elastic modulus, $\langle N \rangle$ is the average number of molecules in the

ensemble, $\langle \delta N^2 \rangle$ its variance, and V the volume of the confined fluid corresponding to the internal diameter.

To compare the bulk moduli obtained from BPR EOS with those from simulations, we focused on the values after capillary condensation, as the bulk modulus presents a linear behavior after reaching condensation when it is expressed in terms of the logarithm of the relative pressure.⁴⁵

Results

The isotherms obtained as a result of the GCMC simulations are shown in Figure 1, from which we calculated the parameters $\delta_{\rm p}$ and $\epsilon_{\rm p}$ using Particle Swarm Optimization, getting $\epsilon_{\rm p}/k_{\rm B}=2080.3\,{\rm K}$, and $\delta_{\rm p}=0.0596\,{\rm nm}$. These parameters were utilized in BPR EOS, and the resulting isotherms are also shown in Figure 1. All the isotherms show good agreement with describing the capillary condensation at all temperatures and pore sizes. However, that is not the case for the adsorbed amount after reaching condensation: The isotherms derived from BPR EOS predict higher densities than those predicted by simulations, which is a known issue for this type of EOS. ⁴⁶ Moreover, GCMC isotherms show increasing density maxima with increasing the pore size, while BPR EOS isotherms for 3 nm in pore size are higher than those of 5 nm in pore size.

From molecular simulations, we obtained the distribution of molecules for each given chemical potential. Figure 2 shows the distribution of molecules in spherical silica pores of 1 nm, 3 nm and 5 nm at the temperature $T=87.3\,\mathrm{K}$ and chemical potential $\mu/k_\mathrm{B}=-1207.9\,\mathrm{K}$, after GCMC equilibration. Figure 2 shows that the molecules for 1 nm pores do not follow a normal distribution. Therefore, GCMC simulations cannot be utilized for calculations of bulk modulus for this pore size. We only performed the modulus calculations for the sizes 3 nm and 5 nm.

Figure 3 shows the bulk modulus calculated from the GCMC data using Eq. 28 and from

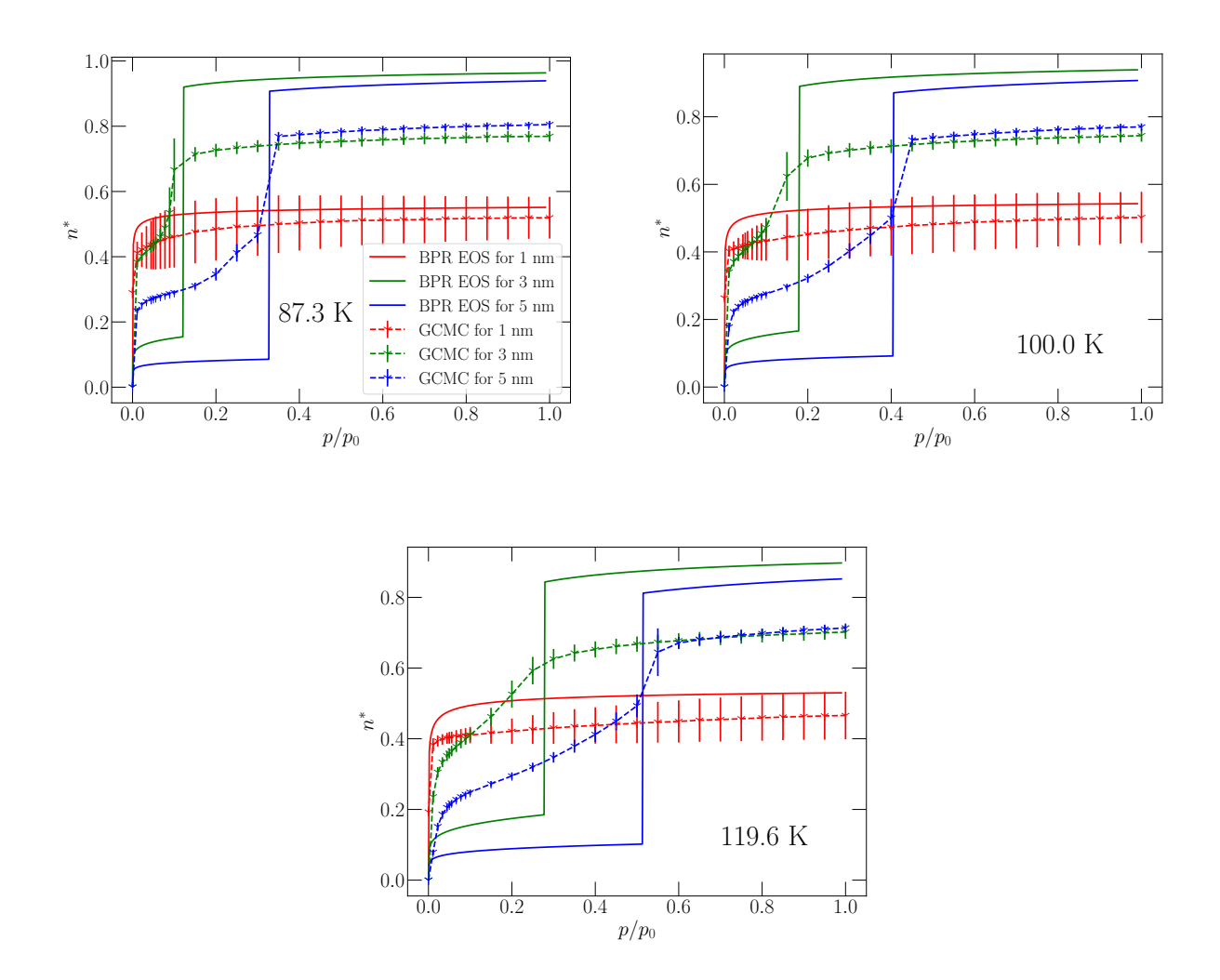


FIGURE 1: Adsorption isotherms of argon predicted by GCMC simulations (dashed curves) and BPR EOS (solid curves) at different temperatures, and for different pore sizes: 1 nm (red curves), 3 nm (green curves), and 5 nm (blue curves). The adsorbed amount is expressed in reduced units ($n^* = n\sigma^3$, where n refers to the confined number density and σ is the fluid-fluid LJ parameter), and related to the relative pressure, where p_0 is the saturation pressure of argon at its respective temperature. The error bars are twice the standard deviation in length.

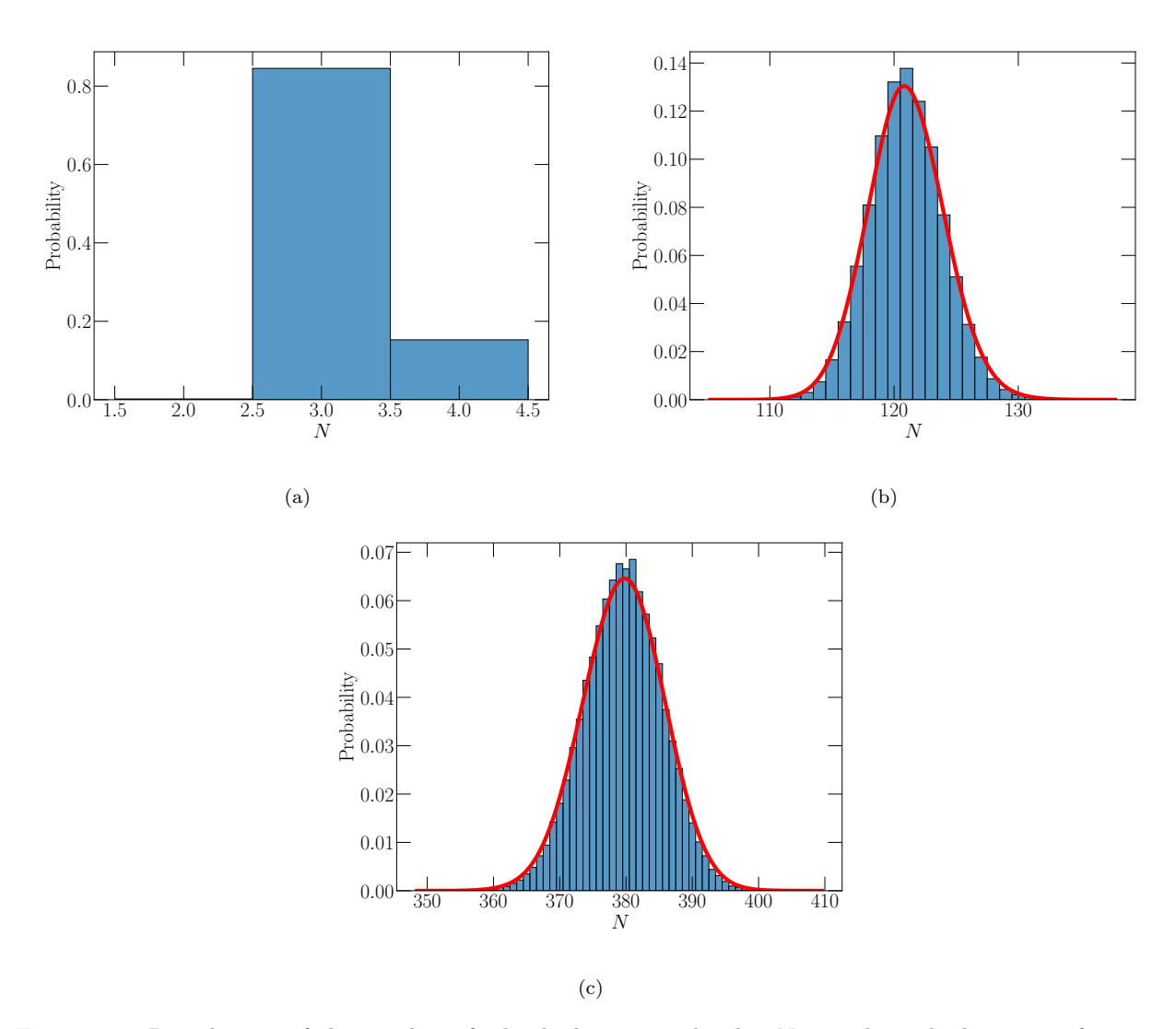


FIGURE 2: Distribution of the number of adsorbed argon molecules N on spherical silica pores for 1 nm (2a), 3 nm (2b), and 5 nm (2c) in pore size at the temperature $T=87.3\,\mathrm{K}$ and chemical potential $\mu/k_\mathrm{B}=-1479.7\,\mathrm{K}$, after performing a GCMC simulation.

BPR EOS using Eq. 13. The modulus is plotted as a function of the Laplace pressure given by

$$P_{\rm L} = \frac{RT}{v_{\rm l}} \ln \left(\frac{p}{p_0} \right), \tag{29}$$

where v_l is the liquid phase molar volume of the bulk fluid at saturation conditions, and it can be obtained experimentally. The results are plotted along with the modulus of bulk liquid argon at the same temperature as a function of the bulk pressure.

Unlike GCMC simulations, BPR EOS permits calculating the bulk modulus even for smaller pore sizes. In Figure 3, the bulk moduli derived from BPR EOS for each pore size follow the Tait-Murnaghan equation⁴⁷ (linear relation between the pressure of the confined fluid and the bulk modulus), where is important to note that the intercepts of each of the lines depend on the pore size. The intercepts for the BPR EOS follow the same trend as those derived from GCMC simulations, but the slopes for 3 nm and 5 nm in pore size differ considerably, especially with the slope of the modulus for bulk argon. Regarding the case of 1 nm, the slope seems to follow a better agreement with the bulk phase. A more detailed explanation of this agreement is shown in the discussion section. The slopes are shown in Table 2.

TABLE 2: Slopes of the bulk moduli (and twice the standard deviations for those obtained from GCMC simulations) derived in Figure 3. The bulk moduli (in MPa) for the bulk phase was obtained by CoolProp.

Pore size	Method	$T = 87.3 \mathrm{K}$	$T = 100 \mathrm{K}$	$T = 119.6 \mathrm{K}$
1 nm	BPR EOS	8.259	7.904	7.288
$3\mathrm{nm}$	GCMC	9.425 ± 0.376	9.701 ± 0.511	10.620 ± 0.540
	BPR EOS	18.446	16.070	14.094
$5\mathrm{nm}$	GCMC	9.856 ± 1.156	10.783 ± 0.357	12.377 ± 0.657
	BPR EOS	16.486	13.972	10.995
Bulk	CoolProp	9.649	9.925	10.555

The bulk modulus at $p = p_0$ was also related to the reciprocal of the pore sizes, which is shown in Figure 4. The bulk moduli derived from BPR EOS predict the linear dependence with the inverse of the pore size until 2 nm in size, even though they do not show a good

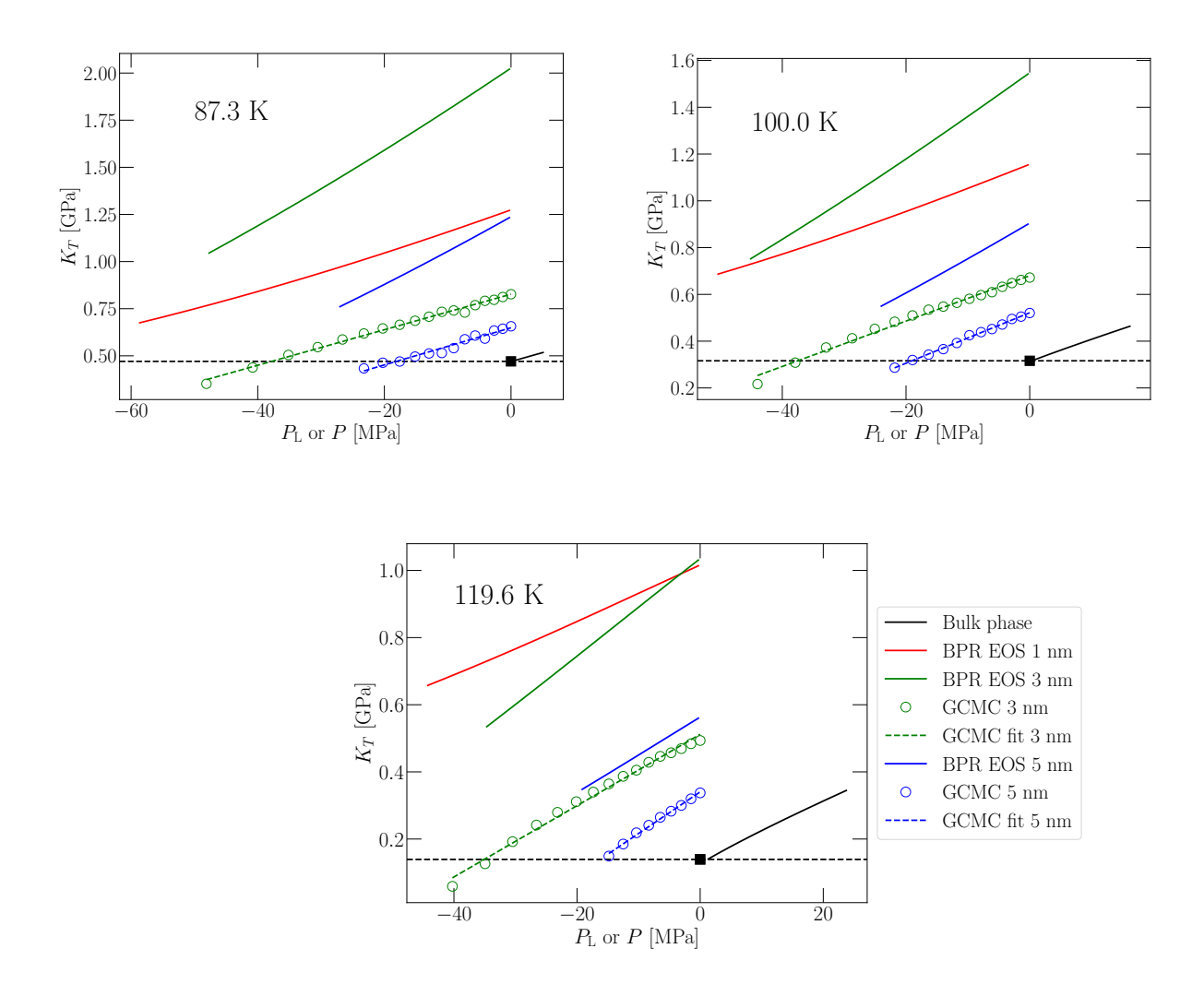


FIGURE 3: Bulk moduli of confined argon in spherical silica pores derived from BPR EOS (solid lines), and GCMC simulations (circles) along with their linear fit (dashed lines) at different temperatures, and for different pore sizes, as well as the modulus of bulk liquid argon. For the confined phase, the bulk modulus is a function of the Laplace pressure (v_l was calculated by CoolProp⁴⁸); for the bulk phase, it is a function of the external pressure. Saturation pressure for the latter is represented by the black square, and the bulk modulus at saturation pressure by the dashed horizontal line.

match with the values obtained from GCMC simulations. When pore size decreases, the moduli predicted by BPR EOS show a minimum around 1.1 nm, maxima around 2 nm and 0.8 nm, and a steeply increase at $d_{\rm ext} = 0.7$ nm.

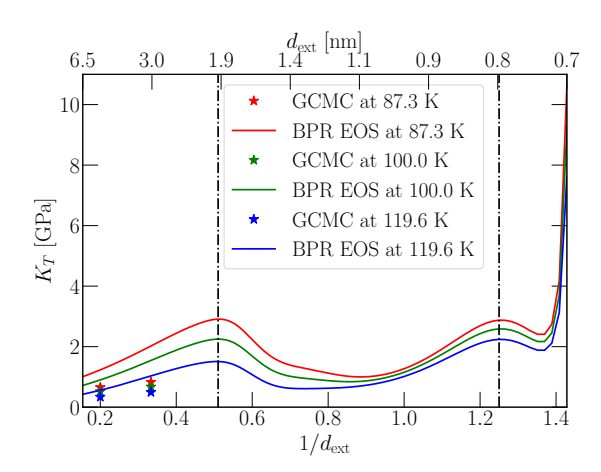


FIGURE 4: Bulk moduli of confined argon in spherical silica pores derived from BPR EOS (solid lines), and GCMC simulations (stars) at the temperatures 87.3 K (red curves), 100 K (green curves), and 119.6 K (blue curves), related to the reciprocal of the pore sizes $1/d_{\rm ext}$ at the saturation pressure of its associated temperature. The vertical dashed-dotted lines point the local maxima of the bulk modulus at 6σ (around $2 \, \rm nm$), and $\frac{3}{4} \pi \sigma$ (around $0.8 \, \rm nm$), where σ is obtained from Eq. 8.

The behavior of $K_{\rm T}$ as a function of the pore size (Fig. 4) can be better understood based on the solvation pressure as a function of the pore size as it is shown in the right-hand side of Figure 5. This time, we split the fluid pressure into two terms: The first one, $p_{\rm ff}$ refers to the pressure derived from PR EOS and is associated with the fluid-fluid interactions; the second term $p_{\rm sf}$ refers to the solid-fluid interactions. Figure 5 also shows that the same behavior was obtained for the bulk modulus, meaning that $p_{\rm ff}$ has a stronger effect on the bulk modulus than $p_{\rm sf}$, which implies the consistency of the bulk modulus of confined fluids with the Tait-Murnaghan equation. For pores smaller than 2 nm (around 6σ), the solid-fluid interactions outweight the $p_{\rm ff}$, affecting the linearity of K_T .

The effect of $p_{\rm sf}$ was previously pointed out by Dobrzanski et al. when they analyzed TvdW EOS for cylinders.²⁶ They found that the pressure term related to the bulk fluid excerpted a strong influence under the solvation pressure, and the reason for the peaks in their elastic moduli as a function of $1/d_{\rm ext}$ was especially caused by the factor $v - b_{\rm p}$. The

left-hand side of Figure 5 shows a correlation between the factor $v/(v-b_p)$ and the reciprocal of the pore size. Around 2 nm, 0.8 nm, and 0.7 nm, the difference $v-b_p$ approaches zero, and $v/(v-b_p)$ reaches its peaks.

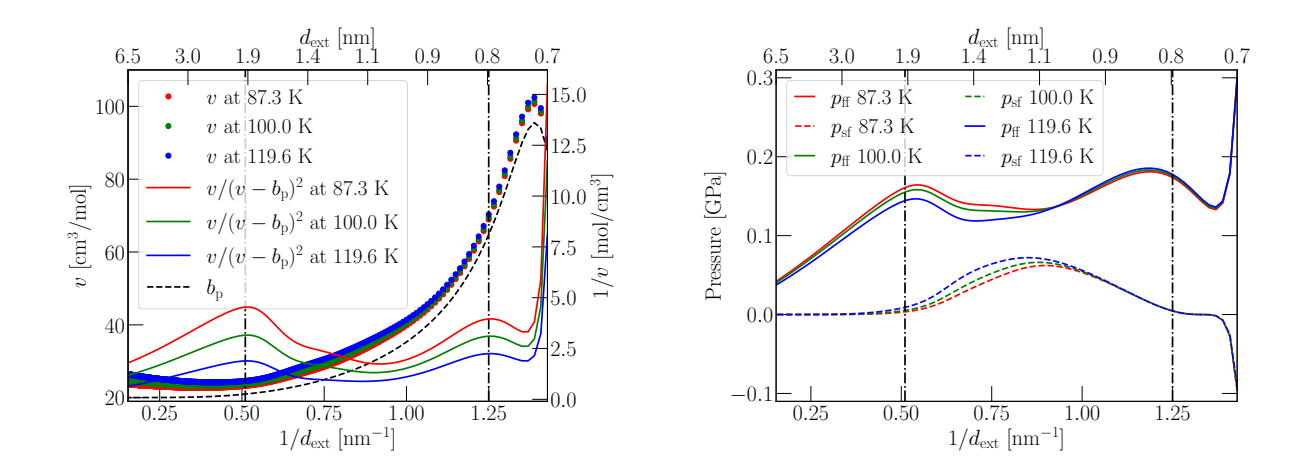


FIGURE 5: Left: Molar volume of confined liquid argon at saturation pressure as a function of the reciprocal of the pore size for each temperature calculated from BPR EOS, and the first term of Eq. 13 (considering only v and $b_{\rm p}$). Calculations from BPR EOS. Right: Confined fluid pressure split into fluid-fluid interactions ($p_{\rm ff}$) and solid-fluid interactions ($p_{\rm sf}$) as a function of the pore size at different temperatures. The dashed-dotted lines point the local maxima of the bulk modulus around 2 nm and 0.8 nm.

Discussion

Although there were no quantitative agreements after comparing both methods, BPR EOS and GCMC simulations, the qualitative agreements are remarkable, such as the presence of the capillary condensation, the linear dependence of the bulk modulus with the logarithm of the external pressure and the reciprocal of the pore size (for large pores), and the dependence of the latter on the temperature (as higher the external temperature is as higher external pressures will be needed to condense the fluid). The correct qualitative behavior of pressure and modulus predicted by BPR EOS allows us to analyze the fluids in micropores ($d_{\text{ext}} < 2 \, \text{nm}$) where GCMC fails to calculate the bulk modulus.

There is a hypothesis. The behavior of the bulk modulus in Figure 4 may be a consequence of the molecule distribution in the pore. Figures 5 show that the repulsive fluid-fluid

interactions affect the elastic modulus more than the solid-fluid interactions. When the pore is larger than 6σ (around 2 nm) in external diameter, the distribution of molecules not interacting with the walls tends to follow a normal distribution, as in the bulk fluid. Consequently, the bulk modulus of the confined fluid has approximately the same slope as the modulus of the bulk fluid. However, for micropores, the pore walls force the confined fluid to rearrange its molecules depending on the pore shape, ³⁵ which explains the maximum at $3\pi\sigma/4$ (around 0.8 nm) in external diameter. This rearrangement reduces their movement and causes a solid-like behavior. Consequently, the elastic modulus shows a non-linear trend.

When the pore size is lower than a critical value of 0.8 nm shown in Figure 4, a complete layer of fluid molecules is removed from the pore, giving more freedom to the remaining molecules to move randomly. This explains why the maxima are at $r_p/\sigma \in \{3, 3\pi/8, 1\}$. However, as the pore becomes smaller, the fluid molecules reduce their movement and finally reach once again the solid-like behavior. When the external diameter approaches 2σ , the bulk modulus tends to infinity, and therefore, BPR EOS loses any physical meaning. As a consequence, the linear trend of the bulk modulus doesn't depend on the pore shape for pores larger than 2 nm (or 6σ) in external diameter.

Adsorption-desorption process in mesoporous materials typically shows hysteresis.^{49–51} However, in our work, when studying the modulus of the fluid in the pores, we considered adsorption process only, not calculating the desorption branches of the isotherms. Neglecting the desorption branch and hysteresis when calculating the modulus of confined fluid is justified by multiple ultrasonic experiments on adsorption in mesoporous solids.^{12,52–54} Experimentally the fluid modulus in mesoporous samples can be probed only when pores are completely filled with a capillary condensate, at pressures above the hysteresis region.

While the predictions of EOS considered here did not provide quantitative agreement with the molecular simulation results, we believe that such agreement can be achieved if a more advanced EOS for confined fluid is utilized. In recent years various SAFT-based EOSs for adsorbed fluids demonstrated excellent performance in predicting other thermodynamic

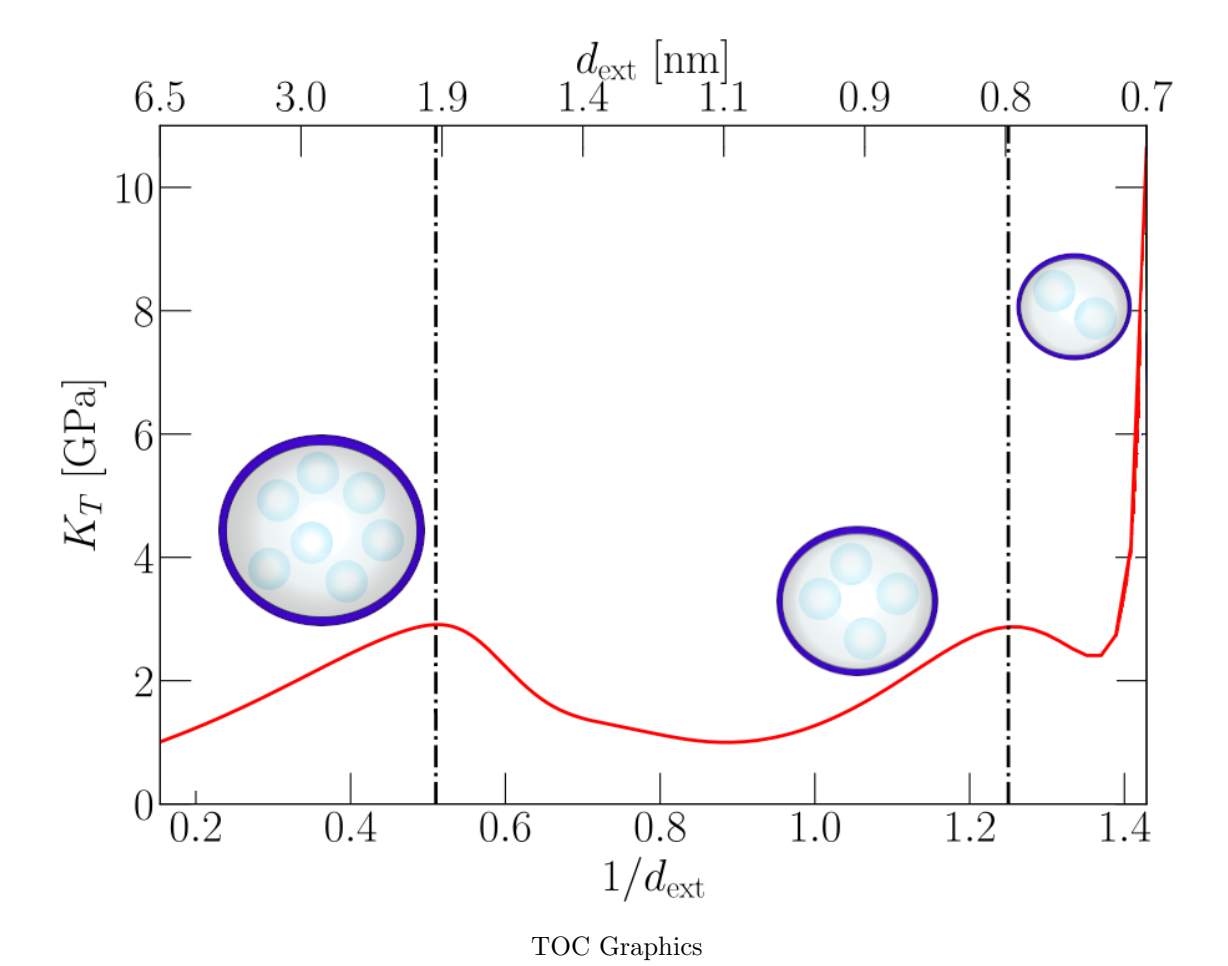
properties .^{55–58} Therefore it is plausible that these equations can provide predictions for elastic properties as well.

Conclusion

To summarize, we derived an analytical expression for the bulk modulus of a fluid confined in a spherical nanopore. We parameterized the EOS based on molecular simulation data for argon in model silica pores and showed that the resulting model predicts the modulus of argon in three different pore sizes at three different temperatures reasonably well. Our equation gives the linear dependence of the modulus on solvation pressure, as well as the linear dependence on the reciprocal pore size. The latter holds only in the mesopore region, but for micropores we see a non-trivial trend. This trend has not been confirmed by molecular simulations because the simulation method we utilized is not capable of predicting the modulus in micropores. Our study showed that although a more advanced EOS gives better predictions than the EOS based on the van der Waals model, the agreement between elasticity predicted based on the BPR EOS and based on molecular simulations is still only qualitative. Overall, our result is a step towards developing an equation of state for confined fluids, which can be used for predictions of elasticity.

Acknowledgments

S.A.F.R thanks Marcos Molina and Dr. Max Maximov for their help to make first steps in this research. This work was supported by the National Science Foundation (Grant CBET-1944495).



References

- (1) Bocquet, L.; Tabeling, P. Physics and technological aspects of nanofluidics. *Lab Chip* **2014**, *14*, 3143–3158.
- (2) Yeo, L. Y.; Friend, J. R. Surface acoustic wave microfluidics. *Annu. Rev. Fluid Mech.* **2014**, *46*, 379–406.
- (3) Renou, R.; Ghoufi, A.; Szymczyk, A.; Zhu, H.; Neyt, J.-C.; Malfreyt, P. Nanoconfined electrolyte solutions in porous hydrophilic silica membranes. J. Phys. Chem. C 2013, 117, 11017–11027.
- (4) Vanzo, D.; Bratko, D.; Luzar, A. Dynamic control of nanopore wetting in water and saline solutions under an electric field. *J. Phys. Chem. B* **2015**, *119*, 8890–8899.
- (5) Pak, A. J.; Hwang, G. S. Molecular insights into the complex relationship between capacitance and pore morphology in nanoporous carbon-based supercapacitors. ACS Appl. Mater. Interfaces 2016, 8, 34659–34667.
- (6) Pham, T. T.; Lemaire, T.; Capiez-Lernout, E.; Lewerenz, M.; To, Q.-D.; Christie, J. K.; Di Tommaso, D.; de Leeuw, N. H.; Naili, S. Properties of water confined in hydroxyapatite nanopores as derived from molecular dynamics simulations. *Theor. Chem. Acc.* 2015, 134, 1–14.
- (7) Islam, A. W.; Patzek, T. W.; Sun, A. Y. Thermodynamics phase changes of nanopore fluids. J. Nat. Gas Sci. Eng. 2015, 25, 134–139.
- (8) Tan, S. P.; Piri, M. Equation-of-state modeling of confined-fluid phase equilibria in nanopores. *Fluid Phase Equilib.* **2015**, *393*, 48–63.
- (9) Alfi, M.; Nasrabadi, H.; Banerjee, D. Experimental investigation of confinement effect on phase behavior of hexane, heptane and octane using lab-on-a-chip technology. *Fluid Phase Equilib.* **2016**, 423, 25–33.

- (10) Salahshoor, S.; Fahes, M.; Teodoriu, C. A review on the effect of confinement on phase behavior in tight formations. *J. Nat. Gas Sci. Eng.* **2018**, *51*, 89–103.
- (11) Yang, G.; Li, X. Modified Peng-Robinson equation of state for CO2/hydrocarbon systems within nanopores. J. Nat. Gas Sci. Eng. 2020, 84, 103700.
- (12) Page, J. H.; Liu, J.; Abeles, B.; Herbolzheimer, E.; Deckman, H. W.; Weitz, D. A. Adsorption and desorption of a wetting fluid in Vycor studied by acoustic and optical techniques. *Phys. Rev. E* **1995**, *52*, 2763.
- (13) Gor, G. Y.; Gurevich, B. Gassmann Theory Applies to Nanoporous Media. *Geophys. Res. Lett.* **2018**, *45*, 146–155.
- (14) Corrente, N. J.; Dobrzanski, C. D.; Gor, G. Y. Compressibility of Supercritical Methane in Nanopores: A Molecular Simulation Study. *Energy & Fuels* **2020**, *34*, 1506–1513.
- (15) Dobrzanski, C. D.; Gurevich, B.; Gor, G. Y. Elastic properties of confined fluids from molecular modeling to ultrasonic experiments on porous solids. Appl. Phys. Rev. 2021, 8, 021317.
- (16) Han, D.-H.; Batzle, M. L. Gassmann's equation and fluid-saturation effects on seismic velocities. *Geophysics* **2004**, *69*, 398–405.
- (17) Yan, F.; Han, D.-H. Effect of pore geometry on Gassmann fluid substitution. *Geophys. Prospect.* **2016**, *64*, 1575–1587.
- (18) Nanda, N. C. Seismic data interpretation and evaluation for hydrocarbon exploration and production; Springer, 2021.
- (19) Martini, A.; Vadakkepatt, A. Compressibility of thin film lubricants characterized using atomistic simulation. *Tribol. Lett.* **2010**, *38*, 33–38.

- (20) Coasne, B.; Czwartos, J.; Sliwinska-Bartkowiak, M.; Gubbins, K. E. Effect of Pressure on the Freezing of Pure Fluids and Mixtures Confined in Nanopores. J. Phys. Chem. B 2009, 113, 13874–13881.
- (21) Gor, G. Y. Adsorption Stress Changes the Elasticity of Liquid Argon Confined in a Nanopore. *Langmuir* **2014**, *30*, 13564–13569.
- (22) Sun, Z.; Kang, Y. Local elastic properties of nano-confined fluids: A density functional study. *Phys. Lett. A* **2014**, *378*, 1739–1745.
- (23) Sun, Z.; Kang, Y.; Li, S. Elastic Properties of Confined Fluids in Nanopores: An Acoustic-Propagation Model. J. Phys. Chem. B 2022, 126, 8010–8020.
- (24) Landers, J.; Gor, G. Y.; Neimark, A. V. Density Functional Theory Methods for Characterization of Porous Materials. *Colloids Surf.*, A **2013**, 437, 3–32.
- (25) Gor, G. Y. *Poromechanics VI*; ASCE, 2017; pp 465–472.
- (26) Dobrzanski, C. D.; Corrente, N. J.; Gor, G. Y. Compressibility of Simple Fluid in Cylindrical Confinement: Molecular Simulation and Equation of State Modeling. *Ind. Eng. Chem. Res.* 2020, 59, 8393–8402.
- (27) Van der Waals, J. D. On the continuity of the gas and liquid state. *Leiden University*, *Leiden, Netherlands* **1873**, 301.
- (28) Schoen, M.; Diestler, D. J. Analytical treatment of a simple fluid adsorbed in a slit-pore. J. Chem. Phys. 1998, 109, 5596–5606.
- (29) Truskett, T. M.; Debenedetti, P. G.; Torquato, S. Thermodynamic implications of confinement for a waterlike fluid. *J. Chem. Phys.* **2001**, *114*, 2401–2418.
- (30) Zarragoicoechea, G. J.; Kuz, V. A. van der Waals equation of state for a fluid in a nanopore. *Phys. Rev. E* **2002**, *65*, 021110.

- (31) Travalloni, L.; Castier, M.; Tavares, F. W.; Sandler, S. I. Thermodynamic modeling of confined fluids using an extension of the generalized van der Waals theory. *Chem. Eng. Sci.* **2010**, *65*, 3088–3099.
- (32) Peng, D.-Y.; Robinson, D. B. A new two-constant equation of state. *Industrial & Engineering Chemistry Fundamentals* **1976**, *15*, 59–64.
- (33) Barbosa, G. D.; D'Lima, M. L.; Daghash, S. M.; Castier, M.; Tavares, F. W.; Travalloni, L. Cubic equations of state extended to confined fluids: New mixing rules and extension to spherical pores. *Chem. Eng. Sci.* **2018**, *184*, 52–61.
- (34) Pfoertner, H. Densest Packing of Spheres in a Sphere. http://www.randomwalk.de/sphere/insphr/ylspheresinsphr.html, 2006; [Online; accessed 19-September-2022].
- (35) Dobrzanski, C. D.; Maximov, M. A.; Gor, G. Y. Effect of pore geometry on the compressibility of a confined simple fluid. *J. Chem. Phys.* **2018**, *148*, 054503.
- (36) Schwaab, M.; Biscaia Jr, E. C.; Monteiro, J. L.; Pinto, J. C. Nonlinear parameter estimation through particle swarm optimization. *Chem. Eng. Sci.* **2008**, *63*, 1542–1552.
- (37) Tuckerman, M. Statistical mechanics: theory and molecular simulation; Oxford university press, 2010.
- (38) McQuarrie, D. A. Statistical Mechanics; Harper & Row: New York, 1976.
- (39) Rasmussen, C. J. Molecular simulation of simple fluids and polymers in nanoconfinement. Ph.D. thesis, Rutgers The State University of New Jersey-New Brunswick, New Brunswick, 2012.
- (40) Ravikovitch, P. I.; Wei, D.; Chueh, W. T.; Haller, G. L.; Neimark, A. V. Evaluation of pore structure parameters of MCM-41 catalyst supports and catalysts by means of nitrogen and argon adsorption. *J. Phys. Chem. B* **1997**, *101*, 3671–3679.

- (41) Vishnyakov, A.; Neimark, A. V. Studies of liquid-vapor equilibria, criticality, and spinodal transitions in nanopores by the gauge cell Monte Carlo simulation method. *J. Phys. Chem. B* **2001**, *105*, 7009–7020.
- (42) Johnson, J. K.; Zollweg, J. A.; Gubbins, K. E. The Lennard-Jones equation of state revisited. *Mol. Phys.* **1993**, *78*, 591–618.
- (43) Baksh, M. S. A.; Yang, R. T. Model for spherical cavity radii and potential functions of sorbates in zeolites. *AIChE J.* **1991**, *37*, 923–930.
- (44) Gor, G. Y.; Rasmussen, C. J.; Neimark, A. V. Capillary Condensation Hysteresis in Overlapping Spherical Pores: A Monte Carlo Simulation Study. *Langmuir* 2012, 28, 12100–12107.
- (45) Gor, G. Y.; Siderius, D. W.; Rasmussen, C. J.; Krekelberg, W. P.; Shen, V. K.; Bernstein, N. Relation Between Pore Size and the Compressibility of a Confined Fluid. J. Chem. Phys. 2015, 143, 194506.
- (46) Gonçalves, A. F.; Castier, M.; Franco, L. F. Capillary condensation: Limitations of the multicomponent potential theory of adsorption (MPTA). Fluid Phase Equilib. 2023, 569, 113759.
- (47) Macdonald, J. R. Some simple isothermal equations of state. Rev. Mod. Phys. 1966, 38, 669.
- (48) Bell, I. H.; Wronski, J.; Quoilin, S.; Lemort, V. Pure and Pseudo-pure Fluid Thermophysical Property Evaluation and the Open-Source Thermophysical Property Library CoolProp. *Ind. Eng. Chem. Res.* **2014**, *53*, 2498–2508.
- (49) Hiratsuka, T.; Tanaka, H.; Miyahara, M. T. Mechanism of Kinetically Controlled Capillary Condensation in Nanopores: A Combined Experimental and Monte Carlo Approach. ACS Nano 2017, 11, 269–276.

- (50) Dantas, S.; Struckhoff, K. C.; Thommes, M.; Neimark, A. V. Phase Behavior and Capillary Condensation Hysteresis of Carbon Dioxide in Mesopores. *Langmuir* 2019, 35, 11291–11298.
- (51) Morishige, K. Revisiting the Nature of Adsorption and Desorption Branches: Temperature Dependence of Adsorption Hysteresis in Ordered Mesoporous Silica. *ACS Omega* **2021**, *6*, 15964–15974.
- (52) Schappert, K.; Pelster, R. Influence of the Laplace pressure on the elasticity of argon in nanopores. *Europhys. Lett.* **2014**, *105*, 56001.
- (53) Maximov, M. A.; Gor, G. Y. Molecular simulations shed light on potential uses of ultrasound in nitrogen adsorption experiments. *Langmuir* **2018**, *34*, 15650–15657.
- (54) Ogbebor, J.; Valenza, J. J.; Ravikovitch, P. I.; Karunarathne, A.; Muraro, G.; Lebedev, M.; Gurevich, B.; Khalizov, A. F.; Gor, G. Y. Ultrasonic Study of Water Adsorbed in Nanoporous Glasses. arXiv preprint arXiv:2303.12193 2023,
- (55) Franco, L. F.; Economou, I. G.; Castier, M. Statistical Mechanical Model for Adsorption Coupled with SAFT-VR Mie Equation of State. *Langmuir* **2017**, *33*, 11291–11298.
- (56) Campos-Villalobos, G.; Ravipati, S.; Haslam, A. J.; Jackson, G.; Suaste, J.; Gil-Villegas, A. Modelling adsorption using an augmented two-dimensional statistical associating fluid theory: 2D-SAFT-VR Mie. Mol. Phys. 2019, 117, 3770–3782.
- (57) Araujo, I. S.; Franco, L. F. A model to predict adsorption of mixtures coupled with SAFT-VR Mie equation of state. *Fluid Phase Equilib.* **2019**, *496*, 61–68.
- (58) Aslyamov, T.; Pletneva, V.; Khlyupin, A. Random surface statistical associating fluid theory: Adsorption of n-alkanes on rough surface. *J. Chem. Phys.* **2019**, *150*, 054703.